Radial Ultrashort TE Imaging Removes the Need for Breath-Holding in Hepatic Iron Overload Quantification by R2* MRI

Aaryani Tipirneni-Sajja[1,2]
Axel J. Krafft[1,3]
M. Beth McCarville[1]
Ralf B. Loeffler[1]
Ruitian Song[1]
Jane S. Hankins[4]
Claudia M. Hillenbrand[1]

Keywords: free breathing, hepatic iron overload, liver MRI, R2* quantification, T2* relaxometry, ultrashort TE imaging

DOI:10.2214/AJR.16.17183

Received July 29, 2016; accepted after revision December 28, 2016.

Supported by grant 5 R01 DK088988 from the National Institute of Diabetes and Digestive and Kidney Diseases of the National Institutes of Health and the American Lebanese Syrian Associated Charities (the fund-raising organization of St. Jude Children's Research Hospital).

Based on a presentation at the Society for Pediatric Radiology and European Society of Paediatric Radiology 2016 international pediatric radiology conjoint meeting and exhibition, Chicago, IL.

[1]Department of Diagnostic Imaging, St. Jude Children's Research Hospital, 262 Danny Thomas Pl, Memphis, TN 38105-3678. Address correspondence to C. M. Hillenbrand (claudia.hillenbrand@stjude.org).

[2]Department of Biomedical Engineering, University of Memphis, Memphis, TN.

[3]Department of Radiology, Medical Physics, Medical Center–University of Freiburg, Faculty of Medicine, Freiburg, Germany.

[4]Department of Hematology, St. Jude Children's Research Hospital, Memphis, TN.

AJR 2017; 209:187–194

0361–803X/17/2091–187

OBJECTIVE. The objective of this study is to evaluate radial free-breathing (FB) multiecho ultrashort TE (UTE) imaging as an alternative to Cartesian FB multiecho gradient-recalled echo (GRE) imaging for quantitative assessment of hepatic iron content (HIC) in sedated patients and subjects unable to perform breath-hold (BH) maneuvers.

MATERIALS AND METHODS. FB multiecho GRE imaging and FB multiecho UTE imaging were conducted for 46 test group patients with iron overload who could not complete BH maneuvers (38 patients were sedated, and eight were not sedated) and 16 control patients who could complete BH maneuvers. Control patients also underwent standard BH multiecho GRE imaging. Quantitative R2* maps were calculated, and mean liver R2* values and coefficients of variation (CVs) for different acquisitions and patient groups were compared using statistical analysis.

RESULTS. FB multiecho GRE images displayed motion artifacts and significantly lower R2* values, compared with standard BH multiecho GRE images and FB multiecho UTE images in the control cohort and FB multiecho UTE images in the test cohort. In contrast, FB multiecho UTE images produced artifact-free R2* maps, and mean R2* values were not significantly different from those measured by BH multiecho GRE imaging. Motion artifacts on FB multiecho GRE images resulted in an R2* CV that was approximately twofold higher than the R2* CV from BH multiecho GRE imaging and FB multiecho UTE imaging. The R2* CV was relatively constant over the range of R2* values for FB multiecho UTE, but it increased with increases in R2* for FB multiecho GRE imaging, reflecting that motion artifacts had a stronger impact on R2* estimation with increasing iron burden.

CONCLUSION. FB multiecho UTE imaging was less motion sensitive because of radial sampling, produced excellent image quality, and yielded accurate R2* estimates within the same acquisition time used for multiaveraged FB multiecho GRE imaging. Thus, FB multiecho UTE imaging is a viable alternative for accurate HIC assessment in sedated children and patients who cannot complete BH maneuvers.

Iron overload is a serious condition that usually arises from increased gastrointestinal absorption of dietary iron (e.g., hereditary hemochromatosis) or from multiple blood transfusions (e.g., for sickle cell disease, β-thalassemia, or myelosuppression during chemotherapy) [1–5]. Because the body has no effective physiologic mechanism for excreting it, iron can accumulate in the liver and other organs, eventually causing organ damage [6, 7]. Iron overload can result in significant morbidity and mortality if it is not effectively monitored and treated [8, 9].

Hepatic iron content (HIC) is a reliable marker for total body iron accumulation [10]. The traditional reference standard for assessing HIC is liver biopsy [11], but this procedure is invasive and painful, has sampling variability [12], and is associated with risks such as bleeding and infection [13]. In recent years, R2* MRI has been increasingly used as a noninvasive alternative to liver biopsy for HIC quantification. R2* MRI is based on a linear correlation between HIC and the tissue-specific MRI relaxation parameter R2* [14–16]. R2* is determined by quantifying the signal decay of a Cartesian multiecho gradient-recalled echo (GRE) sequence typically measured in a single breath-hold (BH). However, breath-holding is not possible for sedated patients and is problematic for patients who have difficulty holding their breath for a short period. Problems with breath-holding can lead to poor image quality caused by respiratory motion artifacts. The artifact signal

may introduce errors in the quantification of R2*-based HIC because calibration equations have been established only for BH examinations of liver tissue void of artifacts.

Several attempts have been made to overcome breathing artifacts in patients who are not able to complete BH maneuvers. Respiratory gating based on external bellows or navigator methods can mitigate breathing artifacts [17–19]. However, such techniques add additional steps and complexity to the clinical workflow, increase the total scan time, and can fail if patients have irregular breathing patterns [20, 21]. Signal averaging is an alternative to respiratory gating and is the most commonly used solution for sedated patients and for young children who cannot hold their breath during thoracic and abdominal imaging [22]. Signal averaging reduces motion artifacts by decreasing the relative contribution of a motion-corrupted signal component compared with the overall signal. However, increasing the number of averages also increases the scan time. Radial sampling techniques are robust to respiratory motion because of oversampling of the center of the *k*-space, which is traversed with every radial projection [23, 24]. Azevedo et al. [25] and Chandarana et al. [26] showed the clinical feasibility of using an FB 3D T1-weighted radial volumetric interpolated BH examination as a viable alternative to abdominal imaging for sedated pediatric patients and patients who are unable to suspend respiration.

In the context of visceral iron quantification, ultrashort TE (UTE) imaging has been proposed for imaging tissues with very short T2 or T2* components [27, 28]. UTE imaging uses half radiofrequency pulse excitations with radial center-out data sampling [27]. Krafft et al. [29] showed the technical feasibility of multiecho UTE imaging for R2* quantification in patients with massive hepatic iron overload (HIC > 25 mg Fe/g of dry liver weight). Because of the radial sampling process, this sequence is relatively insensitive to respiratory motion and thus can potentially overcome the limitations introduced by motion artifacts during R2*-based HIC quantification.

The purpose of this study is to evaluate R2* quantification by radial FB multiecho UTE imaging for sedated patients and for subjects who are not able to complete BH maneuvers. We compare FB multiecho UTE imaging with a commonly used alternative technique: Cartesian FB multiecho GRE imaging with multiple averages. We further compare the liver R2* values obtained using each of the FB methods (FB multiecho GRE imaging and FB multiecho UTE imaging) with the liver R2* values obtained using the conventional Cartesian BH multiecho GRE technique in a control group of patients undergoing R2* MRI for HIC quantification (the group consists only of patients who could complete BH maneuvers).

Materials and Methods

Participants

This retrospective study was approved by the institutional review board of St. Jude Children's Research Hospital. Data were collected from patients who underwent MRI for HIC assessment. Patients were retrospectively assigned to either a test cohort or a control cohort. The cohorts were differentiated on the basis of the imaging performed: patients who were unable to complete BH maneuvers underwent FB multiecho GRE and FB multiecho UTE imaging, and patients who were able to complete BH maneuvers underwent BH multiecho GRE, FB multiecho GRE, and FB multiecho UTE imaging.

Test cohort (patients unable to complete BH maneuver)—All test subjects were consecutively recruited from our ongoing institutional MIDAS (Massive Iron Deposit Assessment, National Clinical Trials identifier 01572922 on ClinicalTrials.gov) study during the period from July 2012 to March 2016. A total of 130 patients underwent scanning performed in accordance with the MIDAS protocol during this period. Of these 130 patients, 51 could not complete BH maneuvers and had both FB examinations performed. One dataset could not be processed because of technical issues; therefore, 50 patients (19 male patients and 31 female patients; median [± SD] age, 6.6 ± 7.0 years; range, 1.6–33.1 years) were assigned to the test cohort.

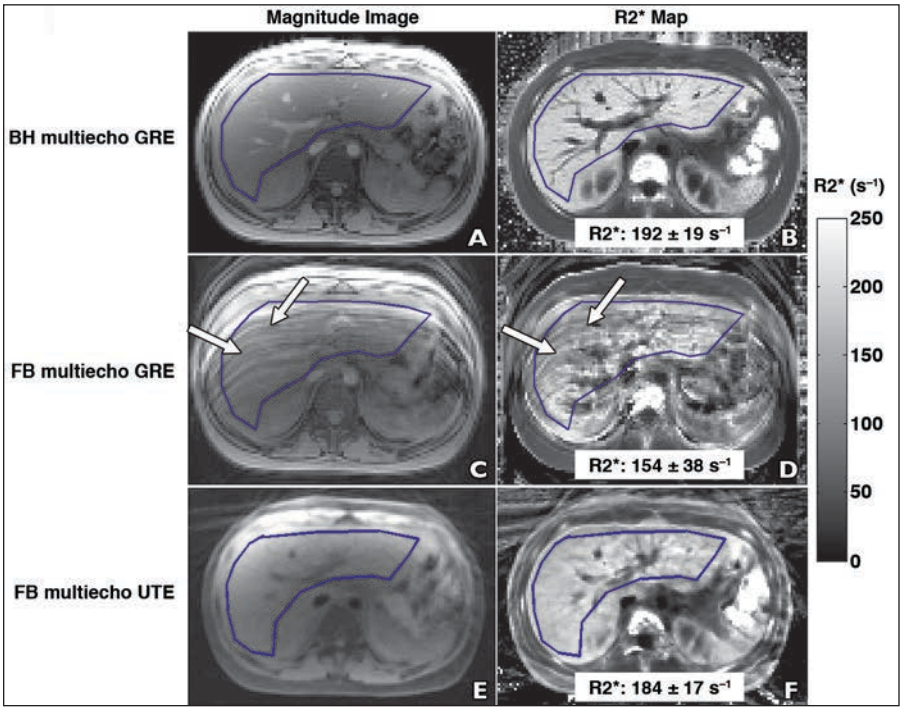

Fig. 1—13-year-old girl with sickle cell disease and mild iron overload who, as control patient, had breath-hold (BH) and free-breathing (FB) MRI sequences compared.
A–**F**, First-echo magnitude MR images of liver (**A**, **C**, and **E**) and respective R2* maps (**B**, **D**, and **F**) acquired by BH multiecho gradient-recalled echo (GRE) (**A** and **B**), FB multiecho GRE (**C** and **D**), and FB multiecho ultrashort TE (UTE) (**E** and **F**) imaging. For each acquisition, mean R2* (± SD) was calculated for whole-liver ROI (*blue outline*, **A**–**F**) after exclusion of blood vessels by histogram analysis. BH multiecho GRE R2* MRI–based hepatic iron content (HIC) of 5.4 mg Fe/g of dry liver weight (calculated using calibration equation in [36]) served as reference standard because existing calibration curves were derived from such examinations. Typical FB multiecho GRE motion artifacts (*arrows*, **C** and **D**) are seen. For FB multiecho GRE acquisition, R2* values are lower and SD is higher than values for BH multiecho GRE and FB multiecho UTE acquisitions. Note that R2* value obtained using FB multiecho UTE imaging is in close agreement with that obtained using BH multiecho GRE imaging, which suggests that FB multiecho UTE acquisition provides accurate results under FB conditions. Applying BH multiecho GRE R2* HIC calibration equation [36] to respective R2* values results in apparent HIC of 4.2 mg Fe/g of dry liver weight for FB multiecho GRE imaging and 5.1 mg Fe/g of dry liver weight for FB multiecho UTE imaging.

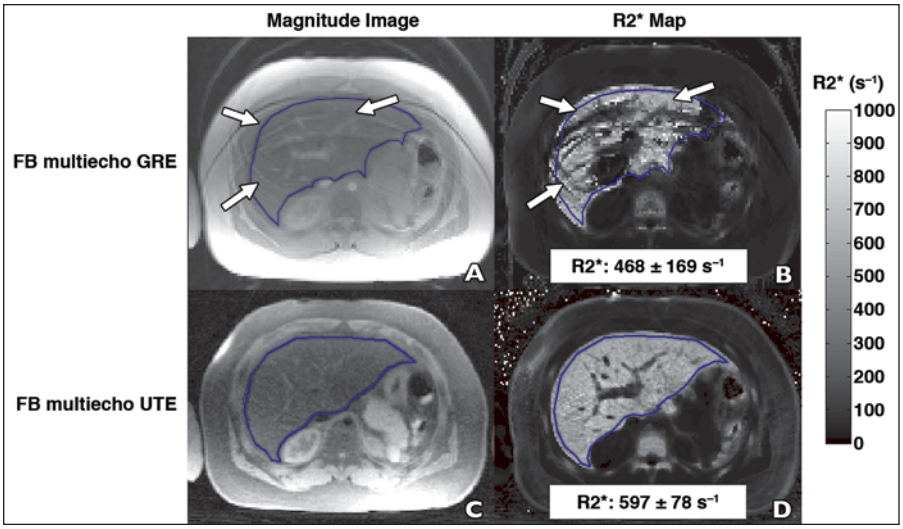

Fig. 2—10-year-old girl with sickle cell disease and high iron overload who was sedated.
A–**D**, First-echo magnitude MR images of liver (**A** and **C**) and respective R2* (**B** and **D**) maps acquired by free-breathing (FB) multiecho gradient-recalled echo (GRE) imaging (**A** and **B**) and FB multiecho ultrashort TE (UTE) imaging (**C** and **D**) show comparison of FB sequences. Mean R2* value (± SD) was calculated for whole-liver ROI (*blue outline*, **A**–**D**) after exclusion of blood vessels by histogram analysis. Motion artifacts (*arrows*) are visible on magnitude image (**A**) and R2* map (**B**) acquired using FB multiecho GRE imaging. Mean R2* value obtained by FB multiecho GRE imaging was lower by 22% and SD was twofold higher, compared with FB multiecho UTE imaging. In contrast, FB multiecho UTE (**C** and **D**) images were cleaner than FB multiecho GRE images (**A** and **B**), with only minor residual streaking artifacts from radial sampling. FB multiecho UTE R2* map (**D**) shows better representation of portal vein than does FB multiecho GRE R2*map (**B**). Applying BH multiecho GRE R2* hepatic iron content (HIC) calibration equation [36] to calculated R2* values results in HIC of 17.9 mg Fe/g of dry liver weight for FB multiecho UTE imaging and HIC of 13.9 mg Fe/g of dry liver weight for FB multiecho GRE imaging, which may be indicative of HIC underestimation.

Of the 50 participants, 40 (16 male patients and 24 female patients; median age, 5.9 ± 5.8 years; range, 1.6–33.1 years) received sedation and 10 (three male patients and seven female patients; median age, 11.6 ± 8.2 years; range, 5.9–31.5 years) did not receive sedation but were unable to complete BH maneuvers. Diagnoses included sickle cell disease (n = 28), β-thalassemia major (n = 6), Diamond-Blackfan anemia (n = 3), acute myeloid leukemia (n = 2), severe aplastic anemia (n = 1), acute lymphocytic leukemia (n = 5), Wilms tumor (n = 1), adrenocorticocarcinoma (n = 1), Langerhans cell histiocytosis (n = 1), myelodysplastic syndrome (n = 1), and severe combined immunodeficiency (n = 1).

The use of sedation is governed by institutional policies and is usually offered to patients younger than 7 years. After the MRI procedure has been discussed, the decision to sedate is made jointly by referring clinicians, child life specialists, and the patient, legal guardian, or both. All nonsedated patients were asked to comply with the BH maneuvers during multiecho GRE image acquisition. If the MRI technologists saw motion artifacts on the acquired BH images, they repeated acquisition several times. If severe motion artifacts were still visible, then the patient was asked to relax and take shallow breaths, and FB multiecho GRE imaging with multiple averages was then performed. The reasons for BH failure were not documented by the technologists; however, the patient group was frail and often had signs of sleepiness and exhaustion, regardless of age.

Control cohort (patients able to complete BH maneuver)—From September 2015 to March 2016, control data were consecutively collected from patients undergoing standard diagnostic MRI for HIC assessment at St. Jude Children's Research Hospital. A total of 16 consecutive patients (six male patients and 10 female patients; median age, 16.2 ± 5.8 years; range, 10.8–32.9 years) did not receive sedation, were BH compliant (for approximately 21 seconds), and completed all three examinations (one BH and two FB examinations), and they therefore qualified for inclusion in this

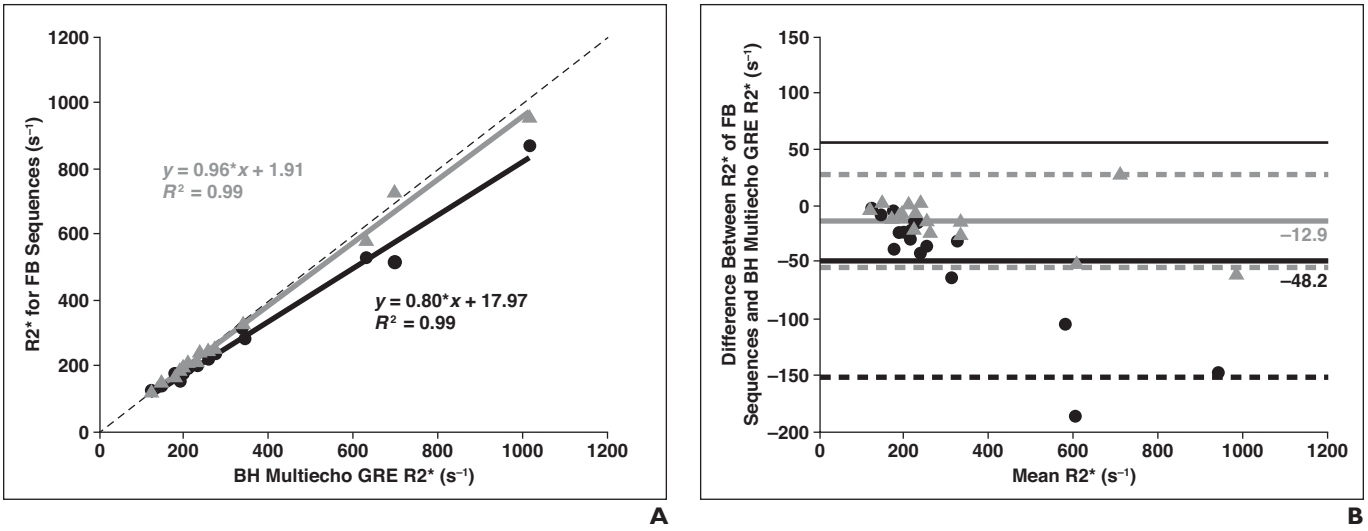

Fig. 3—Mean liver R2* values obtained using different MRI acquisitions in control cohort.
A and **B**, In linear regression plot (**A**) and Bland-Altman plot (**B**), circles denote data for patients who underwent FB multiecho gradient-recalled echo MRI, and triangles denote data for patients who underwent FB multiecho ultrashort TE imaging. In regression plot (**A**), solid lines denote regression lines for data points, and dashed line denotes unity line. In Bland-Altman plot (**B**), solid lines denote mean bias, and dashed lines denote 95% CIs (± 2 SD). Regression equations, correlation coefficients (R^2), and mean biases for different comparisons are also included in plots.

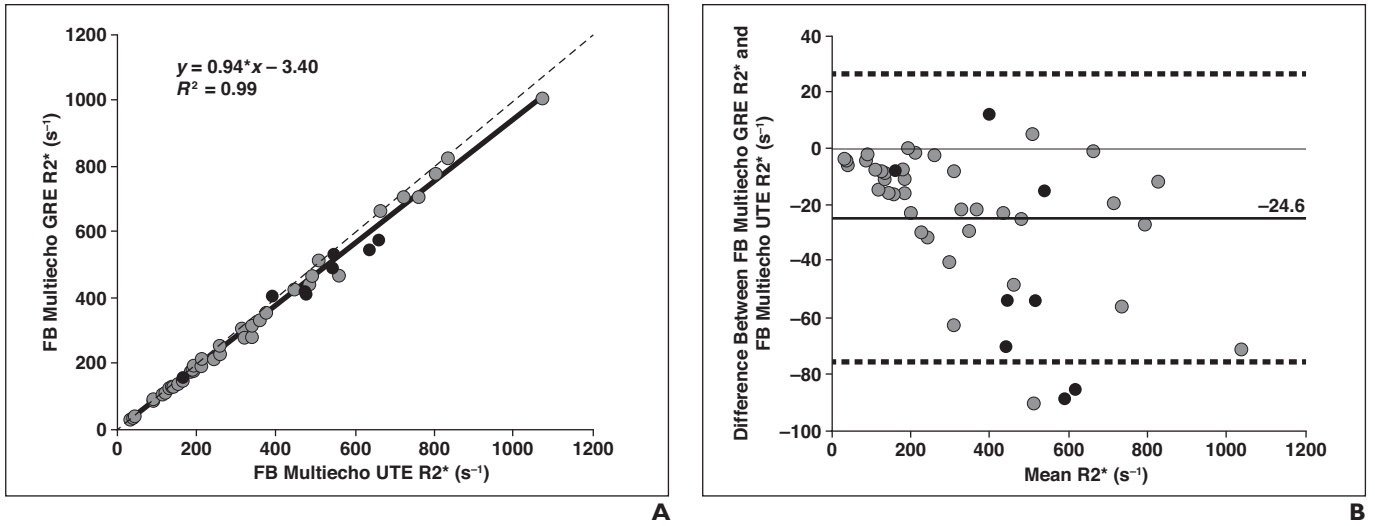

Fig. 4—Mean liver R2* values obtained using free-breathing (FB) multiecho gradient-recalled echo (GRE) and FB multiecho ultrashort TE (UTE) MRI acquisitions in test cohort. **A** and **B,** In both linear regression plot (**A**) and Bland-Altman plot (**B**), gray circles denote sedated patients, and black circles denote nonsedated patients. In regression plot (**A**), solid line denotes regression line for entire test cohort (both sedated and nonsedated patients), and dashed line denotes unity line. Regression plot (**A**) also includes regression equation and correlation coefficient (R^2) for regression analysis. In Bland-Altman plot (**B**), thick solid line denotes mean bias and dashed lines represent 95% CIs (± 2 SD); mean bias value is also shown. Within test cohort, regression equation was $y = 0.96*x - 5.55$, $R^2 = 0.99$, and mean bias was –20.2 s^{-1} for sedated group, whereas regression equation was $y = 0.83*x + 37.62$, $R^2 = 0.96$, and mean bias was –45.4 s^{-1} for nonsedated group.

retrospective study. Diagnoses included sickle cell disease ($n = 9$), β-thalassemia major ($n = 3$), acute myeloid leukemia ($n = 2$), and acute lymphocytic leukemia ($n = 2$).

MRI Scans

MRI scans were obtained using a 1.5-T MRI scanner (Magnetom Avanto, Siemens Healthcare) with body and spine array coils used for signal reception. All scans were obtained on a single transverse slice at the location of the main portal vein of the liver. The sequence parameters used for the acquisition of BH multiecho GRE images were as follows: TR/TE_1, 200/1.1 ms; echo spacing 0.8 ms; 20 echoes; bipolar readout gradient; matrix size, 128 × 104 (readout × phase-encoding direction); slice thickness, 10 mm; pixel bandwidth, 1950 Hz/pixel; flip angle, 35°; and scan time, 21 seconds.

FB multiecho GRE image acquisitions were performed using the same imaging parameters used for the acquisition of BH multiecho GRE images, but three to five averages were used, resulting in a scan time of 63–105 seconds. The FB multiecho UTE sequence was applied with three interleaved echo trains (shifted by a change in TE increment of 0.5 ms), in accordance with the method described by Krafft et al. [29]. Sequence parameters used for the FB multiecho UTE sequences were as follows: TR/TE_1, 52.5/0.1 ms; echo spacing, 1.8 ms; 12 echoes per interleave; 192 radial lines; flip angle, 20°; slice thickness, 10 mm; pixel bandwidth, 780 Hz/pixel; and scan time, 60 seconds. For the FB multiecho UTE acquisition, two spatial saturation bands were placed parallel to the imaging slice (gap between saturation band and imaging slice, 10 mm; saturation band thickness, 100 mm) to eliminate out-of-slice signal contributions, and chemically selective saturation radiofrequency pulses were applied to reduce radial streaking artifacts [29]. The readout FOV for all acquisitions ranged from 250 to 500 mm with phase FOV of 68–81%, depending on patient body size. The FOV for FB multiecho UTE imaging was 100 mm larger than the readout FOV for FB multiecho GRE imaging, to match the voxel sizes.

To test for the presence of fat in the liver, an additional multiecho GRE sequence (obtained with the following parameters: TR/TE_1, 200/1.1 ms; echo spacing, 1.4 ms; 20 echoes; matrix size, 128 × 104; slice thickness, 5 mm; pixel bandwidth, 1950 Hz/pixel; flip angle, 45°; and scan time, 21 seconds) with a monopolar readout gradient was also acquired at the same slice location in both the control and test cohorts.

Presence of Hepatic Fat, R2 Mapping, and Image Analysis*

The present study focused on quantifying R2* as a surrogate marker for HIC in patients with iron overload. However, R2* quantification is affected by the presence of fat [30]. Therefore, all patients were tested for hepatic steatosis by applying a published auto-regressive moving-average algorithm for fat-water quantification [31, 32] to the acquired multiecho GRE data before further R2* analysis was conducted. The algorithm was implemented using Matlab (version 8.1, MathWorks). Cases with a fat fraction of 5% or more (i.e., steatosis grade 1 or higher [33]) were excluded from R2* comparisons.

For all acquisitions across both cohorts, quantitative R2* maps were calculated using Matlab. On a pixel-by-pixel basis, the signal decay was fitted to a monoexponential decay by use of a nonlinear least-squares fit method, which accounts for bias caused by Rician noise [34, 35]. To quantify mean liver R2* values, an ROI encompassing the whole liver in the acquired axial slice was manually drawn, and blood vessels were excluded by histogram analysis for each patient, as detailed elsewhere [36, 37]. Because the FOV used for multiecho UTE imaging is larger than that used for multiecho GRE imaging, the ROIs were drawn separately for multiecho GRE and multiecho UTE images. However, outlining the whole liver is simple and straightforward because it is guided by the outer borders of the liver; hence, the variability between the ROIs for both acquisitions would be negligible.

Statistical Analyses

Statistical analysis was performed using a scientific data analysis and graphing software (SigmaPlot, version 12.0, Systat Software) and Matlab. The mean (± SD) and range of R2* values across different acquisitions and patient groups were determined. For the test cohort, the mean R2* values between the two FB acquisitions were compared using the Wilcoxon signed rank test for significant differences. For the control group, because there were three different acquisitions, mean R2* values were first tested for statistically significant differences with the use of repeated measures ANOVA, followed by the Tukey test for pairwise multiple comparisons. No adjustment was made for age and sex between groups because the statistical analysis focused on R2* accuracy and precision between acquisition methods, not between groups, for individual patients.

TABLE 1: Liver R2* Values for Different MRI Acquisitions and Patient Cohorts

	Control Cohort			Test Cohort			
				Sedated		Nonsedated	
Liver R2* Value	BH Multiecho GRE	FB Multiecho GRE	FB Multiecho UTE	FB Multiecho GRE	FB Multiecho UTE	FB Multiecho GRE	FB Multiecho UTE
Mean ± SD (s^{-1})	332 ± 243	284 ± 196[a]	319 ± 233	312 ± 244[a]	332 ± 254	442 ± 370[a]	488 ± 398
Range (s^{-1})	123–1018	122–870	120–956	31–1004	34–1075	158–576	166–662

Note–The mean R2* values were compared for breath-hold (BH) multiecho gradient-recalled echo (GRE), free-breathing (FB) multiecho GRE, and FB multiecho ultrashort TE (UTE) acquisitions in the control cohort, by use of the repeated measures ANOVA, and for FB multiecho GRE and FB multiecho UTE acquisitions in the test cohort, by use of the Wilcoxon signed rank test.

[a]R2* values for FB multiecho GRE imaging were significantly different from those for standard BH multiecho GRE and FB multiecho UTE imaging in the control cohort and from those for FB multiecho UTE imaging in the test cohort.

Furthermore, for analysis of accuracy, linear regression and Bland-Altman analysis were performed for R2* values obtained using different sequences in both cohorts, to quantitatively test for R2* bias introduced by respiratory motion artifacts. For analysis of precision, the coefficient of variation (CV), which was calculated by dividing the SD by the mean R2* value, was compared between different acquisitions in both cohorts to assess the dispersion of the R2* measurements. This two-step approach eliminated the need for a qualitative assessment that encompassed grading of image quality by a radiologist, thereby avoiding intra- and interobserver variability. For all statistical tests, a statistical significance level of $p = 0.05$ was used.

Results

Of the 50 test patients who could not complete the BH maneuver, four (two were sedated and two were not sedated) had grade 1 hepatic steatosis (fat fraction, 5.4–30.5%) and were excluded from analysis. The final cohort consisted of 16 control patients who were able to complete the BH maneuver and 46 test patients (17 male patients and 29 female patients; median age, 6.6 ± 5.6 years; range, 1.6–31.5 years) who were not able to complete the BH maneuver (38 were sedated and eight were not sedated).

In both cohorts, FB multiecho GRE images showed motion artifacts and also quantitatively showed poorer image quality (i.e., a larger SD of the R2* value) than did the FB multiecho UTE images. As an example, Figure 1 shows magnitude images of the liver and the respective R2* maps of BH multiecho GRE, FB multiecho GRE, and FB multiecho UTE acquisitions from a control patient with mild iron overload (R2*-based HIC from BH multiecho GRE acquisition, 5.4 mg Fe/g of dry liver weight). FB multiecho GRE images showed substantial motion (ghosting) artifacts that spanned the entire liver parenchyma, a lower mean liver R2* value, and a higher SD compared with standard BH multiecho GRE images (R2*, 154 s^{-1} ± 38 s^{-1} vs 192 s^{-1} ± 19 s^{-1}, respectively). In contrast, the FB multiecho UTE images had no motion artifacts and only mild blurring, and the mean liver R2* and SD were close to those noted with the use of the standard BH multiecho GRE sequence. Similarly, Figure 2 shows images and respective R2* maps from a sedated child with high iron overload (> 15 mg Fe/g of dry liver weight). FB multiecho GRE images showed that breathing motion resulted in many arclike artifacts that obscured the underlying anatomy and translated into an erroneous R2* map, whereas FB multiecho UTE images showed only minimal streaking artifacts and thus produced a clean R2* map. In this case, the mean liver R2* value calculated by FB multiecho GRE acquisition was 22% lower than that calculated by FB multiecho UTE acquisition, which would directly translate to an underestimation of approximately 4 mg Fe/g of dry liver weight in the high R2* range, according to linear R2* HIC conversions [16, 36].

Table 1 summarizes the range and mean R2* values for different acquisitions and patient groups. With the use of repeated measures ANOVA, the mean liver R2* values from FB multiecho GRE imaging were statistically significantly lower in the control cohort than were those from standard BH multiecho GRE imaging and FB multiecho UTE imaging ($p < 0.05$), whereas the mean liver R2* values from FB multiecho UTE imaging were not statistically significantly different from the values from BH multiecho GRE imaging. Similarly, in the test cohort, the mean liver R2* values from FB multiecho GRE imaging were significantly lower than those from FB multiecho UTE imaging ($p < 0.05$), by use of the Wilcoxon rank test for both the sedated and nonsedated subgroups of patients.

Figures 3 and 4 show the results of linear regression and Bland-Altman analysis of mean liver R2* values obtained by different acquisitions for the control and test cohorts. In the control cohort, the mean liver R2* values from FB multiecho UTE imaging were in close agreement with those from BH multiecho GRE imaging, with a slope of 0.96 and a mean bias of –12.9 s^{-1}. In contrast, R2* values from FB multiecho GRE imaging were underestimated, with a slope of 0.8 and a mean bias of –48.2 s^{-1}, compared with those of BH multiecho GRE imaging. Similarly, in the test cohort, the mean R2* values measured by FB multiecho GRE imaging were consistently lower than those measured by FB multiecho UTE imaging, with a mean bias of –24.6 s^{-1}. Within the test cohort, the underestimation of R2* values is greater for nonsedated patients (slope, 0.83; mean bias, 45.4 s^{-1}) than for sedated patients (slope, 0.96; mean bias, –20.2 s^{-1}).

Figure 5 shows scatterplots of the mean R2* values and CV R2* values measured using different acquisition techniques in the control and test cohorts. For the control cohort, the mean R2* CV for FB multiecho GRE imaging (25.9% ± 8.6%) was almost double that for BH multiecho GRE imaging (15.4% ± 5.5%), whereas it is even lower for FB multiecho UTE imaging (11.1% ± 3.1%). Likewise, for the test cohort, the mean R2* CV for FB multiecho GRE imaging (18.7% ± 6.4%) was double that for FB multiecho UTE imaging (9.6% ± 2.7%). Also, within the test cohort, the mean R2* CV for FB multiecho GRE imaging was higher for the nonsedated subgroup than for the sedated subgroup. For both cohorts, the R2* CV for FB multiecho UTE imaging was relatively constant over the entire range of R2* values, but the R2* CV for FB multiecho GRE imaging increased with an increase in R2* values.

Discussion

The accurate quantification of hepatic R2* values is essential in guiding the man-

agement of patients with iron overload. R2*-based HIC assessment was useful for deciding when to initiate iron chelation therapy, and, more importantly, it enables the precise modification of ongoing doses in patients with high HIC values. FB multiecho GRE imaging acquisitions are susceptible to motion and exhibit artifacts in the phase-encoding direction that can appear within the liver parenchyma and eventually hamper R2*-based HIC estimation. Our study shows that FB multiecho UTE imaging yields much better image quality and R2* maps than does multiaveraged FB multiecho GRE imaging performed within the same scan time. Furthermore, the R2* values from FB multiecho UTE imaging are in close agreement with those from standard BH multiecho GRE imaging and provide superior accuracy (i.e., a lower CV) when compared with FB multiecho GRE imaging. Hence, FB multiecho UTE imaging could replace FB multiecho GRE imaging for potentially more accurate R2* quantification in patients who are unable to hold their breath during the scan.

In both cohorts, Cartesian FB multiecho GRE images showed substantial motion artifacts, compared with radial FB multiecho UTE images. The motion artifacts were primarily introduced by overlap of the high signal from the subcutaneous abdominal fat and the smearing of blood vessels. Because the R2* value of fat and blood is lower than the R2* value of iron-overloaded liver, the motion artifacts seen on FB multiecho GRE images resulted in significantly lower R2* values than did standard BH multiecho GRE images and FB multiecho UTE images in the control cohort and FB multiecho UTE images in the test cohort. Applying fat suppression techniques such as STIR and chemically selective saturation can reduce the contamination of liver tissue by the overlapped fat signal. However, motion artifacts from the skin, residual subcutaneous fat, and smearing of blood vessels and other organs (e.g., kidneys) into the liver tissue can still corrupt the true liver signal (Fig. 6).

The mean R2* CV for FB multiecho GRE imaging was approximately twofold greater than the mean R2* CVs for BH multiecho GRE imaging and FB multiecho UTE imaging in the control cohort and the mean R2* CV for FB multiecho UTE imaging in the test cohort. This is because of the motion artifacts that promote greater signal variation in the liver, causing increased dispersion (SD) in the calculated R2* values and thus resulting in a higher CV. In the control cohort, the mean R2* CV for FB multiecho UTE imaging is even smaller than that for BH multiecho GRE imaging (especially for R2* > 200 s^{-1}), which might be from shorter TEs and a greater number of echoes for FB multiecho UTE imaging, compared with BH multiecho GRE imaging, that increased the fit accuracy of FB multiecho UTE imaging. The R2* CV for FB multiecho UTE imaging was less than 15% for all patients, with the exception of one patient in each cohort, as a result of heterogeneous iron distribution between the liver lobes. The R2* CV for the FB multiecho UTE acquisition was relatively constant over the entire range of R2* values, but the R2* CV for the FB multiecho GRE acquisition increased with an increase in R2*, thus introducing a higher degree of uncertainty at high HIC values.

Between cohorts, underestimation of the R2* and the R2* CV by FB multiecho GRE imaging was higher in the control cohort (slope, 0.80) than in the test cohort (slope, 0.94). However, in the test cohort, underestimation of R2* for the few patients in the nonsedated subgroup (slope, 0.83) was similar to that for the control cohort, whereas the sedated subgroup showed relatively lower R2* bias (slope, 0.96). This might be for the reason that the patients in the sedated group generally have a shallow breathing pattern because of the effects of sedation and also because of their young age (median age, 5.9 years). In contrast, the nonsedated test sub-

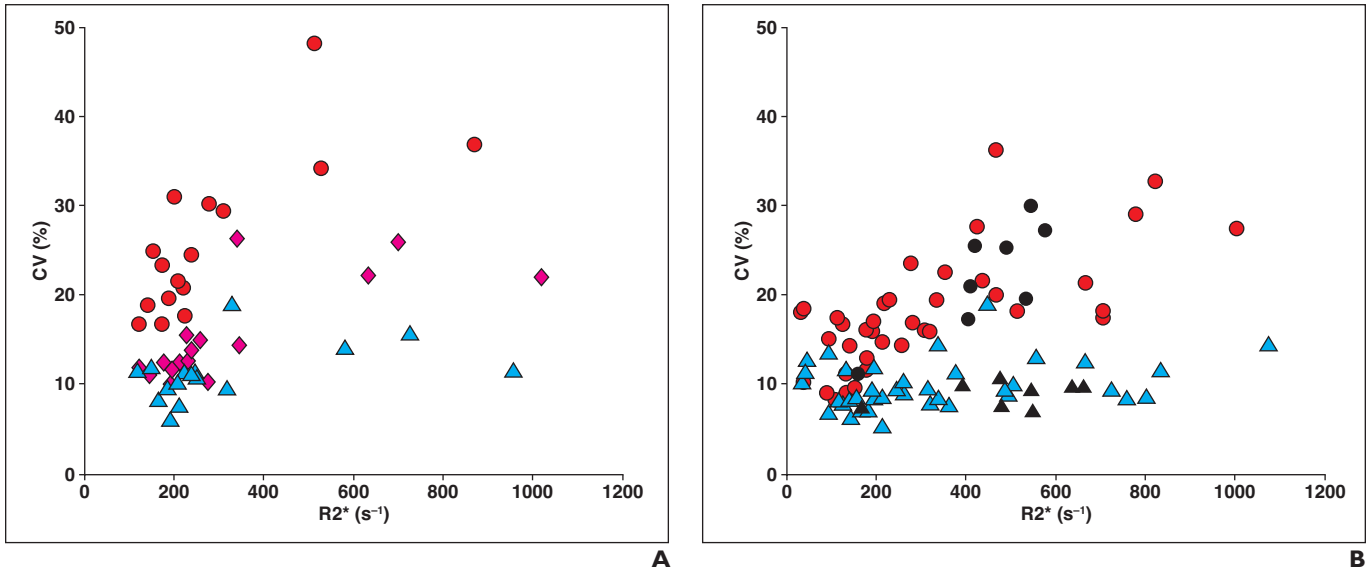

Fig. 5—Coefficients of variation (CVs) of R2* values obtained using different MRI acquisitions in control and test cohorts.
A, Scatterplot for control cohort shows that R2* CV ranged from 10.0% to 26.2% (mean [± SD], 15.4% ± 5.5%) for breath-hold (BH) multiecho gradient-recalled echo (GRE) (*pink diamonds*), 16.7–48.1% (mean, 25.9% ± 8.6%) for free-breathing (FB) multiecho GRE (*red circles*), and 6.0–18.9% (mean, 11.1% ± 3.1%) for FB multiecho ultrashort TE (UTE) (*blue triangles*) imaging.
B, Scatterplot for test cohort shows that R2* CV ranged from 8.2% to 36.2% (mean, 18.7% ± 6.4%) for FB multiecho GRE imaging (*circles*) and from 5.1% to 18.9% (mean, 9.6% ± 2.7%) for FB multiecho UTE imaging (*triangles*). Red circles and blue triangles show data for sedated patients; black circles and black triangles show data for nonsedated patients. Within test cohort, mean R2* CV for sedated and nonsedated subgroups was 18.0% ± 6.4% and 22.1% ± 10.9%, respectively, for FB multiecho GRE, and 9.8% ± 2.7% and 8.9% ± 5.6%, respectively, for FB multiecho UTE. For both test and control cohorts, R2* CV for FB multiecho UTE was relatively constant over entire range of R2* values, whereas R2* CV for FB multiecho GRE increased with increase in R2*.

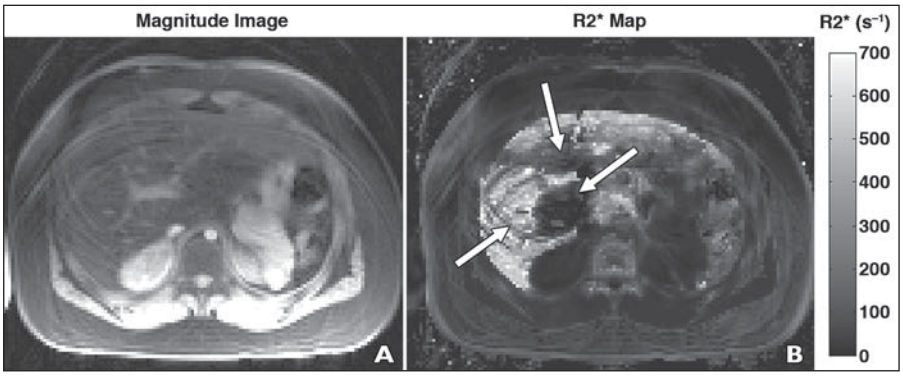

Fig. 6—10-year-old girl with sickle cell disease and high iron overload who was sedated (same patient as in Fig. 2).
A and **B,** First-echo magnitude MR image (**A**) and respective R2* map (**B**) of liver acquired with fat-saturated free-breathing multiecho gradient-recalled echo sequence. Fat was suppressed by applying chemically selective saturation radiofrequency pulses. Although subcutaneous fat signal, which mainly contributed to motion artifacts and R2* bias, was suppressed, motion-induced artifacts (*arrows*) from skin, blood vessels, and kidneys could contaminate liver signal and thereby corrupt R2* quantification.

group and the control cohort comprised relatively older patients with wider chest excursions during breathing and comparatively more subcutaneous fat; this might have led to more pronounced artifacts, R2* underestimation, and a higher R2* CV.

Instead of contouring the entire liver ROI in a cross section, a small ROI in an area devoid of blood vessels and artifacts could be drawn and used for R2* analysis. However, for most patients in the present study, motion artifacts extended over the entire cross section of the liver, so it would have been very difficult to identify an unaffected ROI that was free of artifacts. Moreover, small ROI analysis is potentially more prone to interreviewer variability [36] and is problematic in cases in which the iron distribution is heterogeneous [38, 39].

FB multiecho UTE imaging was less sensitive to motion because of radial sampling. Consequently, radial multiecho GRE techniques should also be useful in the context of minimizing respiratory-induced artifacts under FB. However, apart from radial sampling, another advantage of FB multiecho UTE imaging is that it has TEs shorter than those for standard multiecho GRE acquisitions. Therefore, multiecho UTE imaging allows the measurement of higher R2* values in cases of massive iron overload [29] for which standard Cartesian or radial multiecho GRE acquisitions are unsuccessful [15, 16].

Translation of findings from FB multiecho UTE imaging to clinical practice requires good agreement of R2* values measured by FB multiecho UTE with those measured by the reference BH multiecho GRE method. Our results for the small group of control patients who were able to complete BH maneuvers showed that the mean liver R2* values from FB multiecho UTE imaging were not significantly different from those from BH multiecho GRE imaging, with a slope of 0.96 determined by linear regression. These findings are consistent with earlier findings in phantoms [29].

Our study has some limitations. Manual exclusion of the blood vessels [36] could potentially introduce bias in the R2* evaluation through thresholding for vessels that may present differently in a subject for Cartesian and radial acquisition techniques. Also, to our knowledge, no published calibration studies currently exist that compare multiecho UTE imaging–based hepatic R2* values and HIC values determined from biopsy. However, our study showed that mean liver R2* values acquired with biopsy-calibrated BH multiecho GRE and FB multiecho UTE imaging were fairly similar in the 16 patients who could complete BH maneuvers. Clearly, these findings need to be validated in a larger group of patients.

Furthermore, subtle streaking artifacts resulting from radial undersampling are still visible on FB multiecho UTE images; however, their impact on quantification seems negligible, as can be seen from the comparison with BH multiecho GRE images in the control cohort. There is a small cost for artifact-free FB multiecho UTE imaging–based iron assessment, which has an acquisition time (60 seconds) approximately three times longer than that of BH multiecho GRE acquisition (approximately 21 seconds) because of an interleaved TE scheme for dense sampling of the T2* decay. However, preparation of the patient before the procedure (e.g., providing the patient with breathing instructions) and recuperation after the BH multiecho GRE acquisition can result in a total duration of approximately 1 minute, too. Nevertheless, for patients who can complete the BH maneuver, we recommend the use of conventional BH multiecho GRE for R2* quantification because the existing R2* HIC calibrations are based on equivalent BH multiecho GRE acquisitions. However, for sedated children and for patients who have difficulties holding their breath, FB multiecho UTE acquisitions can be an alternative for accurate R2* quantification because they minimize the uncertainties associated with R2*-based HIC quantification that are introduced by breathing motion. More importantly, FB multiecho UTE images can be acquired within the same scan time required to acquire conventional multiaveraged FB multiecho GRE images without increasing the time that the patients spend on the table.

In conclusion, the results of the present study show that FB multiecho GRE images are susceptible to respiratory-induced motion artifacts. This can lead to lower R2* values and, consequently, R2* HIC underestimation. This underestimation seems to be more prominent, in general, for nonsedated patients who are unable to complete BH maneuvers, compared with sedated patients. R2* HIC underestimation will have a clinical impact by delaying initiation of or prematurely discontinuing iron overload therapy (e.g., iron chelation). FB multiecho UTE acquisitions yield excellent image quality and accurate R2* estimates that are consistent with reference BH multiecho GRE data. Hence, FB multiecho UTE acquisition appears to be a reliable method for R2* HIC assessment in sedated patients or patients who cannot complete BH maneuvers, without having the limitations of conventional FB multiecho GRE acquisitions. FB multiecho UTE imaging may replace FB multiecho GRE imaging for quantitative ascertainment of iron in the liver of patients unable to complete BH scans.

Acknowledgments

We thank Gail Fortner, Karen Wodowski, and Martha Rieman, for patient enrollment; Kamisha Flowers, for the human protection regulatory aspects of the study; and Chris Goode, for MRI data collection. We also thank Vani Shanker for scientific editing.

References

1. Olynyk JK, St Pierre TG, Britton RS, Brunt EM, Bacon BR. Duration of hepatic iron exposure increases the risk of significant fibrosis in hereditary hemochromatosis: a new role for magnetic resonance imaging. *Am J Gastroenterol* 2005; 100:837–841
2. Olivieri NF. Progression of iron overload in sickle cell disease. *Semin Hematol* 2001; 38:57–62
3. Prati D, Maggioni M, Milani S, et al. Clinical and histological characterization of liver disease in patients with transfusion-dependent beta-thalassemia: a multicenter study of 117 cases. *Haematologica* 2004; 89:1179–1186
4. Eng J, Fish JD. Insidious iron burden in pediatric patients with acute lymphoblastic leukemia. *Pediatr Blood Cancer* 2011; 56:368–371
5. Nottage K, Gurney JG, Smeltzer M, Castellanos M, Hudson MM, Hankins JS. Trends in transfusion burden among long-term survivors of childhood hematological malignancies. *Leuk Lymphoma* 2013; 54:1719–1723
6. Harmatz P, Butensky E, Quirolo K, et al. Severity of iron overload in patients with sickle cell disease receiving chronic red blood cell transfusion therapy. *Blood* 2000; 96:76–79
7. Taher AT, Musallam KM, Inati A. Iron overload: consequences, assessment, and monitoring. *Hemoglobin* 2009; 33(suppl 1):S46–S57
8. Brittenham GM. Iron-chelating therapy for transfusional iron overload. *N Engl J Med* 2011; 364:146–156
9. Olivieri NF, Brittenham GM. Iron-chelating therapy and the treatment of thalassemia. *Blood* 1997; 89:739–761
10. Angelucci E, Brittenham GM, McLaren CE, et al. Hepatic iron concentration and total body iron stores in thalassemia major. *N Engl J Med* 2000; 343:327–331
11. Angelucci E, Baronciani D, Lucarelli G, et al. Needle liver biopsy in thalassaemia: analyses of diagnostic accuracy and safety in 1184 consecutive biopsies. *Br J Haematol* 1995; 89:757–761
12. Urru SA, Tandurella I, Capasso M, et al. Reproducibility of liver iron concentration measured on a biopsy sample: a validation study in vivo. *Am J Hematol* 2015; 90:87–90
13. Hoffer FA. Liver biopsy methods for pediatric oncology patients. *Pediatr Radiol* 2000; 30:481–488
14. Anderson LJ, Holden S, Davis B, et al. Cardiovascular T2-star (T2*) magnetic resonance for the early diagnosis of myocardial iron overload. *Eur Heart J* 2001; 22:2171–2179
15. Wood JC, Enriquez C, Ghugre N, et al. MRI R2 and R2* mapping accurately estimates hepatic iron concentration in transfusion-dependent thalassemia and sickle cell disease patients. *Blood* 2005; 106:1460–1465
16. Hankins JS, McCarville MB, Loeffler RB, et al. R2* magnetic resonance imaging of the liver in patients with iron overload. *Blood* 2009; 113:4853–4855
17. Danias PG, McConnell MV, Khasgiwala VC, Chuang ML, Edelman RR, Manning WJ. Prospective navigator correction of image position for coronary MR angiography. *Radiology* 1997; 203:733–736
18. Ehman RL, Felmlee JP. Adaptive technique for high-definition MR imaging of moving structures. *Radiology* 1989; 173:255–263
19. Ehman RL, McNamara MT, Pallack M, Hricak H, Higgins CB. Magnetic resonance imaging with respiratory gating: techniques and advantages. *AJR* 1984; 143:1175–1182
20. McConnell MV, Khasgiwala VC, Savord BJ, et al. Comparison of respiratory suppression methods and navigator locations for MR coronary angiography. *AJR* 1997; 168:1369–1375
21. Morita S, Ueno E, Suzuki K, et al. Navigator-triggered prospective acquisition correction (PACE) technique vs. conventional respiratory-triggered technique for free-breathing 3D MRCP: an initial prospective comparative study using healthy volunteers. *J Magn Reson Imaging* 2008; 28:673–677
22. Chavhan GB, Babyn PS, Vasanawala SS. Abdominal MR imaging in children: motion compensation, sequence optimization, and protocol organization. *RadioGraphics* 2013; 33:703–719
23. Hirokawa Y, Isoda H, Maetani YS, Arizono S, Shimada K, Togashi K. Evaluation of motion correction effect and image quality with the periodically rotated overlapping parallel lines with enhanced reconstruction (PROPELLER) (BLADE) and parallel imaging acquisition technique in the upper abdomen. *J Magn Reson Imaging* 2008; 28:957–962
24. Pipe JG. Motion correction with PROPELLER MRI: application to head motion and free-breathing cardiac imaging. *Magn Reson Med* 1999; 42:963–969
25. Azevedo RM, de Campos RO, Ramalho M, Herédia V, Dale BM, Semelka RC. Free-breathing 3D T1-weighted gradient-echo sequence with radial data sampling in abdominal MRI: preliminary observations. *AJR* 2011; 197:650–657
26. Chandarana H, Block TK, Rosenkrantz AB, et al. Free-breathing radial 3D fat-suppressed T1-weighted gradient echo sequence: a viable alternative for contrast-enhanced liver imaging in patients unable to suspend respiration. *Invest Radiol* 2011; 46:648–653
27. Robson MD, Gatehouse PD, Bydder M, Bydder GM. Magnetic resonance: an introduction to ultrashort TE (UTE) imaging. *J Comput Assist Tomogr* 2003; 27:825–846
28. Chappell KE, Patel N, Gatehouse PD, et al. Magnetic resonance imaging of the liver with ultrashort TE (UTE) pulse sequences. *J Magn Reson Imaging* 2003; 18:709–713
29. Krafft AJ, Loeffler RB, Song R, et al. Quantitative ultrashort echo time imaging for assessment of massive iron overload at 1.5 and 3 Tesla. *Magn Reson Med* 2017 Jan 16 [Epub ahead of print]
30. Sirlin CB, Reeder SB. Magnetic resonance imaging quantification of liver iron. *Magn Reson Imaging Clin N Am* 2010; 18:359–381
31. Taylor BA, Hwang KP, Hazle JD, Stafford RJ. Autoregressive moving average modeling for spectral parameter estimation from a multigradient echo chemical shift acquisition. *Med Phys* 2009; 36:753–764
32. Taylor BA, Elliott AM, Hwang KP, Shetty A, Hazle JD, Stafford RJ. Measurement of temperature dependent changes in bone marrow using a rapid chemical shift imaging technique. *J Magn Reson Imaging* 2011; 33:1128–1135
33. Tang A, Tan J, Sun M, et al. Nonalcoholic fatty liver disease: MR imaging of liver proton density fat fraction to assess hepatic steatosis. *Radiology* 2013; 267:422–431
34. Gudbjartsson H, Patz S. The Rician distribution of noisy MRI data. *Magn Reson Med* 1995; 34:910–914
35. Krafft AJ, Loeffler RB, Song R, et al. Does fat suppression via chemically selective saturation affect R2*-MRI for transfusional iron overload assessment? A clinical evaluation at 1.5T and 3T. *Magn Reson Med* 2016; 76:591–601
36. McCarville MB, Hillenbrand CM, Loeffler RB, Smeltzer MP, Li CS, Hankins JS. Comparison of whole liver and small region-of-interest measurements of MRI liver R2* in children with iron overload. *Pediatr Radiol* 2010; 40:1360–1367
37. Deng J, Rigsby CK, Schoeneman S, Boylan E. A semiautomatic postprocessing of liver R2* measurement for assessment of liver iron overload. *Magn Reson Imaging* 2012; 30:799–806
38. Ambu R, Crisponi G, Sciot R, et al. Uneven hepatic iron and phosphorus distribution in beta-thalassemia. *J Hepatol* 1995; 23:544–549
39. St Pierre TG, Clark PR, Chua-anusorn W, et al. Noninvasive measurement and imaging of liver iron concentrations using proton magnetic resonance. *Blood* 2005; 105:855–861